REPORT DOCUMENTATION PAGE

Form Approved OMB No. 0704-0188

1. REPORT DATE *(DD-MM-YYYY)*	2. REPORT TYPE	3. DATES COVERED *(From - To)*
	Technical Papers	

4. TITLE AND SUBTITLE

5a. CONTRACT NUMBER

5b. GRANT NUMBER

5c. PROGRAM ELEMENT NUMBER

6. AUTHOR(S)

5d. PROJECT NUMBER
2303

5e. TASK NUMBER
M2C8

5f. WORK UNIT NUMBER

7. PERFORMING ORGANIZATION NAME(S) AND ADDRESS(ES)

Air Force Research Laboratory (AFMC)
AFRL/PRS
5 Pollux Drive
Edwards AFB CA 93524-7048

8. PERFORMING ORGANIZATION REPORT

9. SPONSORING / MONITORING AGENCY NAME(S) AND ADDRESS(ES)

Air Force Research Laboratory (AFMC)
AFRL/PRS
5 Pollux Drive
Edwards AFB CA 93524-7048

10. SPONSOR/MONITOR'S ACRONYM(S)

11. SPONSOR/MONITOR'S NUMBER(S)

12. DISTRIBUTION / AVAILABILITY STATEMENT

Approved for public release; distribution unlimited.

13. SUPPLEMENTARY NOTES

14. ABSTRACT

15. SUBJECT TERMS

16. SECURITY CLASSIFICATION OF:			17. LIMITATION OF ABSTRACT	18. NUMBER OF PAGES	19a. NAME OF RESPONSIBLE PERSON
a. REPORT	b. ABSTRACT	c. THIS PAGE			Leilani Richardson
Unclassified	Unclassified	Unclassified	A		19b. TELEPHONE NUMBER *(include area code)* (661) 275-5015

62 separate items are enclosed

C8

MEMORANDUM FOR PR (In-House Publication)

FROM: PROI (TI) (STINFO) 16 Jun 2000

SUBJECT: Authorization for Release of Technical Information, Control Number: **AFRL-PR-ED-TP-2000-129**
S. Tam, M. Fajardo, "CO/pH_2: A Molecular Thermometer"

Fiz. Nizk. Temp (journal entry) **(Statement A)**
(Submission Deadline: 21 July 2000)

1. This request has been reviewed by the Foreign Disclosure Office for: a.) appropriateness of distribution statement, b.) military/national critical technology, c.) export controls or distribution restrictions, d.) appropriateness for release to a foreign nation, and e.) technical sensitivity and/or economic sensitivity.
Comments:_____

Signature _____ Date _____

2. This request has been reviewed by the Public Affairs Office for: a.) appropriateness for public release and/or b) possible higher headquarters review.
Comments: _____

Signature _____ Date _____

3. This request has been reviewed by the STINFO for: a.) changes if approved as amended, b.) appropriateness of distribution statement, c.) military/national critical technology, d.) economic sensitivity, e.) parallel review completed if required, and f.) format and completion of meeting clearance form if required
Comments:_____

Signature _____ Date _____

4. This request has been reviewed by PR for: a.) technical accuracy, b.) appropriateness for audience, c.) appropriateness of distribution statement, d.) technical sensitivity and economic sensitivity, e.) military/ national critical technology, and f.) data rights and patentability
Comments:_____

APPROVED/APPROVED AS AMENDED/DISAPPROVED

_____

LESLIE. S. PERKINS, Ph.D (Date)
Staff Scientist
Propulsion Directorate

CO/pH_2: A Molecular Thermometer

Simon Tam and Mario E. Fajardo*

Propulsion Directorate, US Air Force Research Laboratory,
AFRL/PRSP, Bldg. 8451, Edwards AFB, CA 93524-7680, USA
** email: mario_fajardo@ple.af.mil*

We utilize reversible temperature dependent changes in the IR absorption spectrum of CO molecules isolated in solid parahydrogen (pH_2) to probe bulk temperature changes during rapid vapor deposition. The intensity of a well resolved feature near 2135 cm^{-1} increases monotonically with temperature over the 2 to 5 K range. The thermally populated initial state of this transition lies ≈ 8 K above the CO/pH_2 ground state. During the deposition of ≈ 100 ppm CO/pH_2 samples, we detect temperature gradients ~ 10 K/cm in ~ 0.1 cm-thick samples subjected to heat loads ~ 10 mW/cm^2. The resulting estimated thermal conductivity (TC) is 3(±2) mW/cm-K, averaged over the 2 to 5 K region. This value is ~ 1000 times lower than the TC of single crystal solid pH_2, and ~ 10 times lower than previously measured for pH_2 solids doped with 100 ppm concentrations of heavy impurities [Manzhelii, Gorodilov, and Krivchikov, Low Temp. Phys. 22, 131 (1996)]. We attribute this abnormally low TC to the known mixed fcc/hcp structure of the rapid vapor deposited solids.

PACS numbers:

1. INTRODUCTION

The solid molecular hydrogens (SMH, *i.e.*, H_2 and its isotopomers) have been the subject of numerous investigations,[1-8] with both pure and doped systems receiving considerable attention. The production of SMH samples incorporating a homogeneous distribution of isolated dopants is highly problematic, given the vanishingly low solubilities of most species in the liquid hydrogens near their triple points, and the virtually complete further fractionation of these solutions upon freezing. Because of this difficulty, most studies on doped SMH have focused on completely miscible "impurities" such as metastable J=1 rotational states, *e.g.*, orthohydrogen (oH_2) molecules in solid parahydrogen (pH_2), and the six hydrogen isotopomers: H_2, HD, HT, D_2, DT, and T_2.

An alternative method for preparing doped SMH samples is direct gas condensation under conditions precluding the formation of a liquid phase (*i.e.*, reverse sublimation). Condensation of gas mixtures in an enclosed cell

has been used in thermal[9-13] and spectroscopic[6,8,14-25] studies of SMH doped with Ne and heavier impurities. However, to achieve good filling of the cell, and optically transparent solids, cell temperatures must be over ≈ 0.5 of the hydrogen triple point temperature, leading to aggregation of most dopants present at concentrations above a few parts-per-million (ppm). Thus, absent some applicable spectroscopic diagnostic, it is very difficult to know uniquely the state of aggregation of heavy impurities.

Our new Rapid Vapor Deposition method yields millimeters-thick, optically transparent pH_2 solids containing well isolated dopants, even at concentrations ~ 1000 ppm.[26,27] We have applied high resolution infrared (IR) spectroscopy to probe the degree of dopant isolation, and microscopic trapping site structures, in these solids.[24-27] As-deposited samples have a mixed face-centered-cubic/hexagonal-close-packed (fcc/hcp) structure, which anneals almost completely to a polycrystalline hcp structure upon warming to ≈ 5 K. We are interested in how these mixed fcc/hcp and polycrystalline hcp structures affect our samples' thermal and mechanical properties. We also wish to better understand the rapid vapor deposition process; specifically: what is the temperature distribution in the pH_2 solid during a deposition, and how does it influence dopant isolation efficiency?

In what follows, we describe the application of moderate resolution (≈ 1 cm^{-1}) IR absorption spectroscopy to CO/pH_2 solids to begin to answer these questions. While the notion of temperature dependent changes to the IR spectra of hindered rotor dopants in cryogenic solids is certainly not new, we believe our application of this phenomenon to thermometry is novel. An important *caveat* is that our experimental apparatus is designed

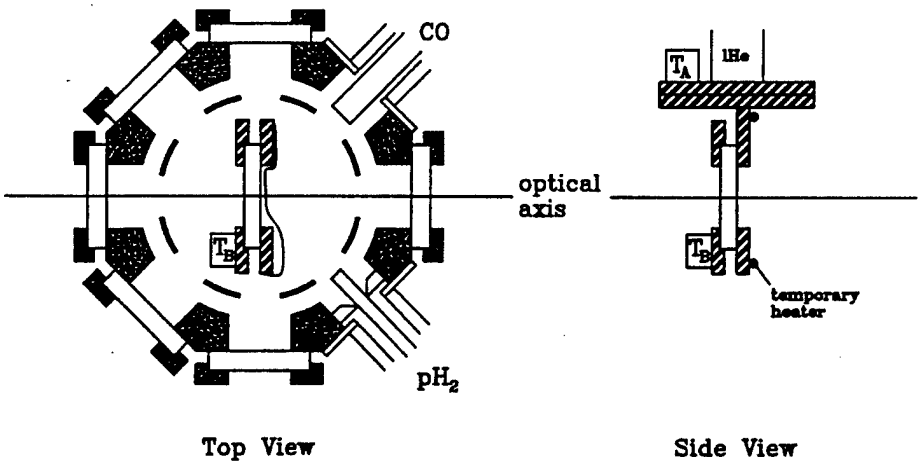

Fig. 1. Experimental Diagram.

for easy optical access to the sample, and *not* for accurate cryogenic thermometry. We intend this report as a demonstration of the advantages of applying combined spectroscopic and thermal diagnostics. We hope that more experienced low temperature experimentalists will recognize these advantages and improve upon our implementation.

2. EXPERIMENTAL

Our experimental apparatus and sample preparation techniques have been described previously.[24-27] Here we concentrate on factors pertaining to the thermal performance of the liquid helium (lHe) bath deposition cryostat. Fig. 1 shows Top and Side views of the sample deposition region. The octagonal outer vacuum shroud has eight o-ring sealed ports for optical access and sample preparation; the liquid nitrogen (lN_2) cooled aluminum radiation shield has matching openings which reduce its effectiveness. The 0.4 cm-thick BaF_2 deposition substrate is clamped in a gold plated oxygen-free-high-conductivity (OFHC) copper holder; all thermal connections are made with 0.01 cm-thick indium foil.

need to reference figure 1 before it is shown

We use two silicon diode sensors to measure the cold tip and deposition substrate temperatures. For calibration purposes, we mount both sensors on the top of the cold tip, remove the substrate holder, and seal the radiation shield openings with aluminum tape. We calibrate the sensors over the 1.5 to 5.0 K range against the lHe bath temperature as calculated from the He vapor pressure[28] measured by two (0-10 torr and 0-1000 torr) capacitance manometers. These capacitance manometers are calibrated against the vapor pressures of water, heptane, hexane, pentane, and butane at 0 °C.[29,30] We estimate the uncertainty in the absolute temperature calibrations as ± 0.1 K (95 % confidence).

The final working locations of the two temperature sensors are best seen in the Side View panel of Fig. 1. The sensor labeled T_A is attached directly to the top of the cryostat cold tip, the T_B sensor is attached to the substrate holder at the furthest point from the cold tip. We routinely report T_B as the "sample temperature" in our spectroscopic studies.

Fig. 1 also shows the location of the temporary electrical heater for calibrating the thermal response of the cryostat. This heater includes a single loop of 0.02 cm meter dia nichrome wire (R = 5.2 Ω) epoxied to the front face of the substrate holder. Connections to the room temperature vacuum feedthrough are made using short 0.02 cm meter dia copper wires (R = 0.5 Ω, including junctions). This arrangement ensures that ≈ 90 % of the electrical power is dissipated in the nichrome heater, but the lack of

thermal anchoring of the copper wires results in an additional ≈ 100 mW heat load on the deposition substrate (*vide infra*).

The CO/pH_2 samples are made by codeposition of metered flows of ≈ 300 K CO gas and (nominally) ≈ 15 K pH_2 gas containing ≈ 100 ppm residual oH_2. As depicted in the Top View panel of Fig. 1, the resulting solids have a variable thickness across the deposition substrate. Although the pressure of uncondensed pH_2 gas remains below ~ 10^{-4} torr, a second pH_2 film forms on the back side of the BaF_2 substrate, amounting to 8.7(± 0.5) % of the main front side film thickness.[31]

IR absorption spectra are obtained using a Fourier Transform spectrometer (capable of 0.1 cm^{-1} resolution) equipped with a glowbar source, a KBr beamsplitter, and a lN_2 cooled HgCdTe detector. The IR beam interrogates a ≈ 0.3 cm dia. cylindrical volume of the pH_2 solid, centered on the BaF_2 substrate. The sample thickness at this point is determined from the intensities of the pH_2 $Q_1(0)+S_0(0)$ or $S_1(0)+S_0(0)$ bands.[31] We estimate the CO concentration from the IR absorptions as described previously,[32] using a value of 60 km/mol for the integrated molecular absorption coefficient.[33] In our CO/pH_2 experiments, these spectroscopically measured concentrations are a factor of 1.35(±0.1) higher than those calculated from the inlet quantities of CO and H_2 gases.

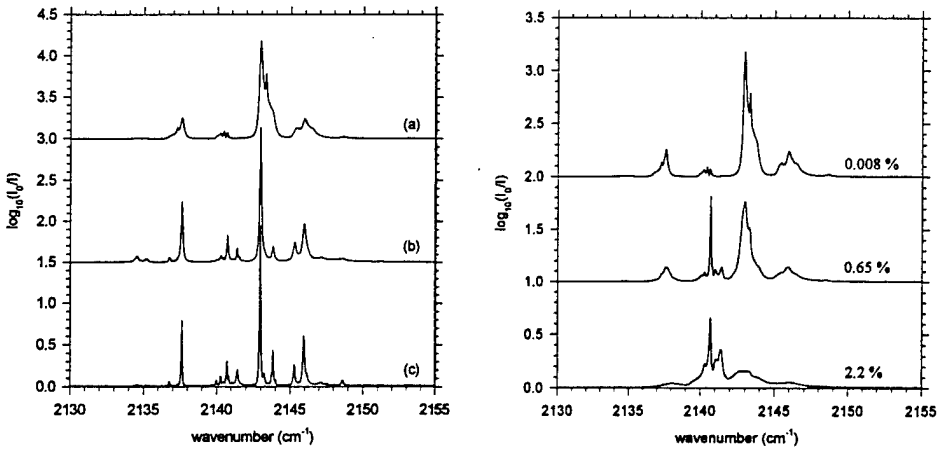

Fig. 2. IR absorption spectra of CO/pH_2 solids at 0.1 cm^{-1} resolution. The left panel is for an 80 ppm CO/pH_2 sample that is 0.17 cm-thick; (a) as-deposited at T_B = 2.4 K, (b) warmed to T_B = 4.8 K, (c) re-cooled to T_B = 2.4 K. The right panel is for three different as-deposited CO/pH_2 samples at T_B = 2.4 K, each containing ≈ 6 μmol of CO. The sample thicknesses are: 0.008 % (0.17 cm), 0.65 % (20 μm), 2.2 % (4.7 μm).

3. RESULTS AND DISCUSSION

reference figure 2 before it is shown

Fig. 2 shows the effects of annealing, and of dopant concentration, on the IR absorption spectra of CO/pH_2 solids. Preliminary analysis of the spectra in the left panel indicates that CO molecules exist in solid pH_2 as slightly hindered rotors, with a rotational constant reduced to ≈ 80 % of the gas phase value (a detailed analysis is still in progress, and will be reported elsewhere[34]). We tentatively assign the complex absorption pattern in trace (2c) to isolated CO molecules in the annealed hcp solid pH_2. It suffices here to note that the features near 2135 cm^{-1} are absorptions from a thermally populated CO hindered rotor state. The right panel of Fig. 2 shows the growth of absorption features near 2141 cm^{-1} with increasing CO dopant concentration; we assign these features to CO dimers and larger clusters. We conclude from these spectra that the

reference to table 1?

Table I. CO/pH_2 thermometer experimental protocol. Entry format is: (a) amount of CO deposited, (b) amount of pH_2 deposited, (c) CO concentration, (d) estimated layer thickness, and (e) duration of each deposition stage. The total pH_2 thickness includes films deposited on both front and back sides of the BaF_2 substrate; other values are calculated assuming a front side layer thickness of 0.92 times the total pH_2 thickness.

expt.#	entry	pH_2 spacer	CO/pH_2 layer	pH_2 overlayer	total pH_2
1	CO:	0	5.9 μmol	0	
	pH_2:	72 mmol	34 mmol	0	106 mmol
	C_{CO}:	0	235 ppm	0	
	d:	0.094 cm	0.044 cm	0	0.150 cm
	t:	41 min	18 min	0	
2	CO:	0	3.7 μmol	0	
	pH_2:	137 mmol	59 mmol	0	196 mmol
	C_{CO}:	0	85 ppm	0	
	d:	0.179 cm	0.077 cm	0	0.278 cm
	t:	41 min	18 min	0	
3	CO:	0	7.3 μmol	0	
	pH_2:	161 mmol	72 mmol	0	233 mmol
	C_{CO}:	0	135 ppm	0	
	d:	0.202 cm	0.091 cm	0	0.319 cm
	t:	41 min	18 min	0	
4	CO:	0	6.5 μmol	0	
	pH_2:	0	52 mmol	136	188 mmol
	C_{CO}:	0	170 ppm	0	
	d:	0	0.070 cm	0.183 cm	0.275 cm
	t:	0	18 min	41 min	

overwhelming majority of CO molecules exist as isolated monomers in ~ 100 ppm CO/pH_2 samples.

Table I shows the experimental protocol for the CO/pH_2 thermometer experiments. We perform four experiments in total: the first three involve the deposition of a pure pH_2 spacer layer prior to the CO/pH_2 deposition; in the fourth (control) experiment the CO/pH_2 layer is deposited first and then covered by a pure pH_2 layer. We record IR absorption spectra covering each 18 minute CO/pH_2 codeposition period, and then again during temperature cycling of the samples. We define the normalized integrated absorbance of the thermometer peak, A_{2135}, as:

$$A_{2135} \equiv \frac{\int_{2133.4}^{2135.8} \log_{10}(I_0/I)\, d\bar{\nu}}{\int_{2133}^{2153} \log_{10}(I_0/I)\, d\bar{\nu}} \qquad (1)$$

Fig. 3 shows the raw spectral data, and a plot of A_{2135} vs. T_B, from expt. #2. The spectra (b) - (k) were obtained after the deposition was

spell out or define 'expt' in 1st mention of paper

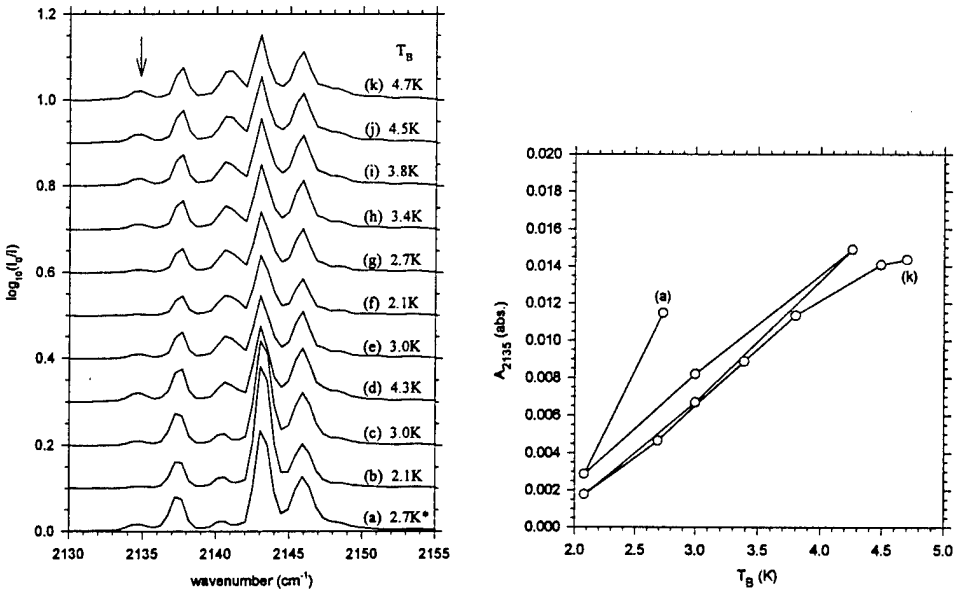

Fig. 3. Temperature dependence of "thermometer peak" at 2135 cm^{-1}. The left panel shows absorption spectra recorded at 1.0 cm^{-1} resolution during ~~expt.~~ #2. spell out Trace (a) was obtained during the deposition of the CO/pH_2 layer and has been re-scaled by a multiplicative factor of two. The right panel shows a plot of the integrated intensities of the thermometer peak (A_{2135}) vs. T_B.

completed. We note that A_{2135} is much larger during the deposition, see point (a), than expected from the measured value of T_B. We attribute this to the existence of a thermal gradient in the pH_2 solid due to the extra heat load during deposition. We also note that points (b) - (d) appear to fall above the trend established by the post-annealing data. We believe this is related to the conversion of fcc regions to hcp upon first annealing.

The left panel of Fig. 4 shows all the post-deposition A_{2135} vs. T_B data from all four experiments, and our fit to a Boltzmann equation:

$$A_{2135} = N \exp(-E/T_{CO}) \qquad (2)$$

in which: E is the energy of the initial state of the 2135 cm^{-1} transition, T_{CO} is the temperature of the CO/pH_2 layer, and N is a normalization constant. A direct nonlinear least-squares fit of the *post-annealing* data to this form yields our best values of E = 7.896 K and N = 0.08602 (a line fit to a plot of $\ln(A_{2135})$ vs. $1/T_{CO}$ yields E = 8.18 K and N = 0.092). We see no systematic deviations from the fit for any particular experiment, thus we conclude that T_B is a reasonable measure of the post-deposition sample temperature, independent of the pH_2 sample thickness. We do note that the *pre-annealing* data appear to fall ≈ 0.4 K lower than the fit; we will account for this potential systematic error, later.

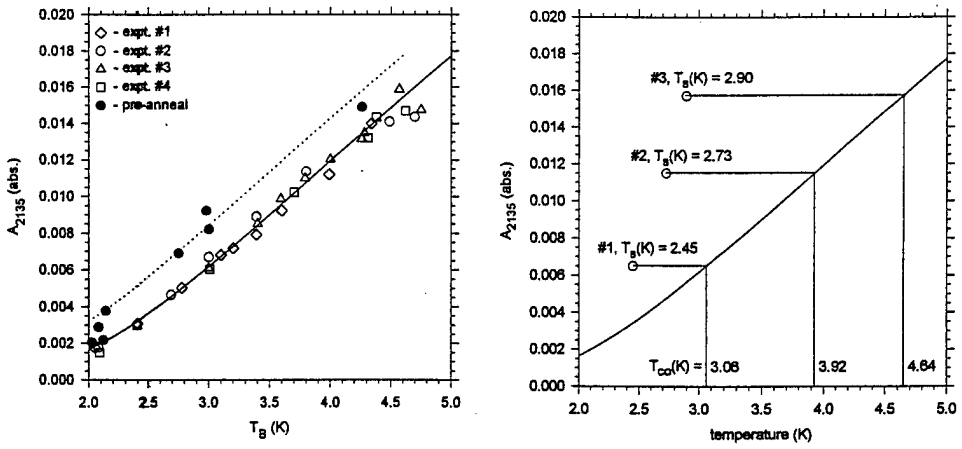

Fig. 4. Fitting and reading the thermometer curve. The left panel shows all the post-deposition data; the closed circles show A_{2135} values obtained from un-annealed samples, the open symbols are data from annealed samples. The solid line is the least squares fit of Eqn. (2) to the post-annealing data; the dotted line is this fit shifted by -0.4 K. The right panel shows T_{CO} values during sample depositions as estimated from the A_{2135} data.

reference for Table II?

Table II. CO/pH_2 thermometer experimental results. Values given are measured before any pH_2 has been deposited, during the CO/pH_2 co-deposition stage, and after the entire sample deposition process has been completed.

pre-deposition		during CO/pH_2 co-deposition			after sample deposition		
expt.#	T_B (K)	T_B (K)	A_{2135}	T_{CO} (K)	T_B (K)	A_{2135}	T_{CO} (K)
1	1.88	2.45	0.0065	3.06	2.03	0.0021	2.13
2	1.90	2.73	0.0115	3.92	2.08	0.0029	2.33
3	1.90	2.90	0.0157	4.64	2.14	0.0038	2.53
4	1.89	2.70	0.0045	2.68	2.12	0.0022	2.15

continue discussion of Fig 4 before figure is shown

The right panel of Fig. 4 depicts how measured values of A_{2135} are converted to T_{CO}; the values obtained by inverting Eqn. (2) are reported in Table II. We note that both T_B and T_{CO} grow with increasing pH_2 deposition rate in the experimental sequence: #1 → #2 → #3. At the highest pH_2 inlet flow rate, ≈ 240 mmol/hr in expt. #3, T_B has increased by ≈ 1.0 K from the pre-deposition base temperature, and T_{CO} shows an additional ≈ 1.7 K rise across the bulk of the ≈ 0.3 cm-thick pH_2 sample.

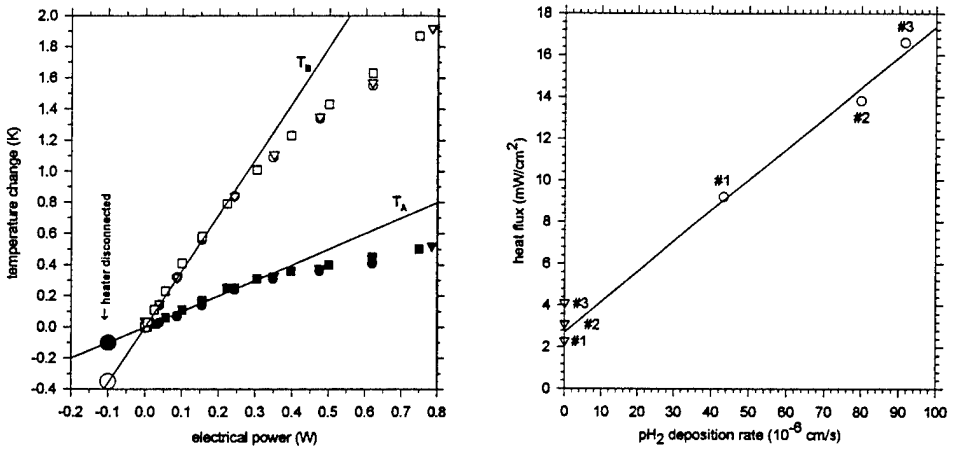

Fig. 5. Calibration of the cryostat's thermal response, and resulting estimated heat loads. The left panel shows a plot of T_A (closed symbols) and T_B (open symbols) vs. dissipated electrical power. The large circles show the base temperatures prior to the addition of the electrical heater. The right panel shows the estimated heat loads during (circles) and after (triangles) the sample depositions vs. the pH_2 deposition rate.

We also note that during the control, expt. #4, the differences between T_B and T_{CO} are not statistically significant. Thus, we can safely neglect the Kapitza resistance[35-38] at the pH_2/BaF_2 interface relative to the thermal resistance through the bulk of the solid pH_2 spacer layer.

discuss Figs before shown

The left panel of Fig. 5 shows the results of our efforts to quantify the heat loads responsible for these observed temperature rises by use of a temporary electrical heater. The lines through the low power T_A and T_B data have slopes of 1.0 and 3.6 K/W, respectively. The increases in base values of T_A and T_B due to thermal conduction through the heater's electrical connections fit onto the extrapolation of these same lines, assuming a 100 mW conduction heat load.

Further assuming a value of A = 17 cm^2 (the area of one side of the deposition substrate holder) we can convert the observed temperature rises [$\Delta T = T_B - T_B$(pre-deposition)] into estimated heat fluxes during and after the pH_2 depositions, as shown in the right panel of Fig. 5. The straight line is a fit to the data obtained *during* the first three CO/pH_2 depositions only. The slope of this line is 140 J/cm^3, which implies the dissipation by the cryostat of 3.3 kJ/mol of pH_2 deposited. This value is much larger than the lower limit of ≈ 1.1 kJ/mol set by the sum of the vaporization energy[5] of pH_2 at 15 K and the heat released in cooling to 4 K. Since we do not monitor the temperature of the pH_2 gas after it leaves the ortho/para converter, we cannot be sure of the source of the additional heating. The non-zero y-intercept of the linear fit coincides with the average of the heat fluxes calculated from the post-deposition increases in base values of T_B. These offsets in T_B also scale (roughly) with increasing sample thickness, consistent with their being due to absorption of room temperature black body radiation by the pH_2 solid. Their absolute magnitudes suggest the absorption of about 10% of the black body radiation available at wavelengths longer than 14 μm. remove space

In principle, we can now estimate the thermal conductivity (TC), κ, of the pH_2 solids by using Fourier's Law:

$$\dot{Q}/A = -\kappa \Delta T/\Delta x \qquad (3)$$

in which: $\dot{Q}/A$ is the heat flux per unit area during each deposition, ΔT is the measured temperature difference across the pH_2 solid, and Δx is the effective thickness of the pH_2 solid. In practice, we find that there are still a number of arbitrary assumptions to be made which will affect the calculated TC values; we will attempt to combine these arbitrary choices to yield upper and lower bounds on the TC values.

Table III shows intermediate quantities and the final results of our TC calculations. To calculate an appropriate separation between the CO/pH_2

Table III. Thermal conductivity calculations. Units: $\dot{Q}/A$ (mW/cm^2), κ (mW/cm-K).

expt.#	Δx(cm)	ΔT_{max}(K)	ΔT_{min}(K)	$(\dot{Q}/A)_{max}$	$(\dot{Q}/A)_{min}$	κ_{min}	κ_{max}
1	0.108	0.61	0.21	9.2	6.9	1.2	4.7
2	0.203	1.19	0.79	13.8	10.7	1.8	3.5
3	0.232	1.74	1.34	16.6	12.5	1.7	2.9

layer and the BaF_2 substrate, we note that not all of the deposited CO contributes equally to the IR absorption spectrum. The CO molecules deposited at the very beginning contribute for the entire acquisition period, whereas those deposited at the very end do not contribute at all. Thus, for Δx we use the sum of the thickness of the pure pH_2 spacer layer plus one-third of the thickness of the CO/pH_2 layer. This factor of 1/3 is the position of the time-weighted centroid of the CO/pH_2 layer:

$$\bar{x} \equiv \frac{\int xydx}{\int ydx} = \frac{\int_0^a x(1-x/a)dx}{\int_0^a (1-x/a)dx} = a/3 \qquad (4).$$

We use two sets of values for the temperature drop across the pH_2 bulk: $\Delta T_{max} = T_{CO} - T_B$, and $\Delta T_{min} = \Delta T_{max} - 0.4$ K to account for the possible systematic error in reading T_{CO} caused by the mixed fcc/hcp structure of the as-deposited solids. We also use two sets of values for the estimated heat fluxes: $(\dot{Q}/A)_{max}$ are the values plotted as open circles in the right panel of Fig. 5, $(\dot{Q}/A)_{min}$ are those values minus the (isotropic) post-deposition radiative heat fluxes plotted as the open triangles. We combine all these values to yield lower and upper estimates for the TCs:

$$\kappa_{min} = -(\dot{Q}/A)_{min} / (\Delta T_{max}/\Delta x) \qquad (5)$$

$$\kappa_{max} = -(\dot{Q}/A)_{max} / (\Delta T_{min}/\Delta x) \qquad (6)$$

We summarize these results as: $\kappa(pH_2) = 3(\pm 2)$ mW/cm-K, averaged over the 2 to 5 K temperature range. This value is ~ 1000 times smaller than the TC of a pure pH_2 single crystal, and about 10 times smaller than reported for doped pH_2 solids.[9-13] We attribute these abnormally low TC values to the mixed fcc/hcp structure of our as-deposited solids.

4. SUMMARY AND FUTURE DIRECTIONS

We have combined IR absorption spectroscopy with cryogenic thermometry to probe the microscopic structures and macroscopic thermal properties of CO-doped pH_2 solids. The main strength of our approach is its ability to establish the state of aggregation of the CO dopants in our samples. The main weakness is our inability to quantify all the heat sources operating on our samples. We are presently considering the possibility of extending our techniques to measurement of the thermal conductivities of annealed samples. We hope that this study will encourage other researchers to incorporate spectroscopic diagnostics into their thermal measurements, wherever possible.

ACKNOWLEDGMENTS

We thank Prof. T. Momose for his analysis of the spectroscopy of the CO/pH_2 system, and Prof. J. Rutledge for valuable discussions concerning the Kapitza conductance.

REFERENCES

1. R.D. McCarty, *Hydrogen Technological Survey--Thermophysical Properties,* NASA-SP-3089, Washington DC (1975).
2. I.F. Silvera, *Rev. Mod. Phys.* **52**, 393 (1980).
3. J. Van Kranendonk, *Solid hydrogen: theory of the properties of solid H_2, HD, and D_2*, Plenum Press, New York (1983).
4. P.C. Souers, *Hydrogen properties for fusion energy*, U. of California Press, Berkeley, (1986).
5. B.I. Verkin, ed., T.B. Selover, Jr., ed. english edition, *Handbook of properties of condensed phases of hydrogen and oxygen*, Hemisphere Publishing, New York (1991).
6. T. Oka, *Annu. Rev. Phys. Chem.* **44**, 299 (1993).
7. V.G. Manzhelii and Y.A. Freiman, eds., *Physics of Cryocrystals*, Springer-Verlag, New York (1996).
8. T. Momose and T. Shida, *Bull. Chem. Soc. Jpn.* **71**, 1 (1998).
9. T.N. Antsygina, B.Y. Gorodilov, N.N. Zholonko, A.I. Krivchikov, V.G. Manzhelii, and V.A. Slyusarev, *Fiz. Nizk. Temp.* **18**, 417 (1992), [*Sov. J. Low Temp. Phys.* **18**, 283 (1992).
10. B.Y. Gorodilov, A.I. Krivchikov, V.G. Manzhelii, and N.N. Zholonko, *Fiz. Nizk. Temp.* **20**, 78 (1994), [*Sov. J. Low Temp. Phys.* **20**, 66 (1994)].
11. B.Y. Gorodilov, A.I. Krivchikov, V.G. Manzhelii, N.N. Zholonko, and

(initial) upper case for titles

O.A. Korolyuk, *Fiz. Nizk. Temp.* **21**, 723 (1995), [*Sov. J. Low Temp. Phys.* **21**, 561 (1995)].
12. M.I. Bagatskii, I.Y. Minchina, and V.G. Manzhelii, *Fiz. Nizk. Temp.* **22**, 52 (1996), [*Low Temp. Phys.* **22**, 37 (1996)].
13. V.G. Manzhelii, B.Y. Gorodilov, and A.I. Krivchikov, *Fiz. Nizk. Temp.* **22**, 174 (1996), [*Low Temp. Phys.* **22**, 131 (1996)].
14. T. Momose, M. Miki, M. Uchida, T. Shimizu, I. Yoshizawa, and T. Shida, *J. Chem. Phys.* **103**, 1400 (1995).
15. T. Momose, M. Uchida, N. Sogoshi, M. Miki, S. Masuda, and T. Shida, *Chem. Phys. Lett.* **246**, 583 (1995).
16. M. Miki, T. Wakabayashi, T. Momose, and T. Shida, *J. Phys. Chem.* **100**, 12135 (1996).
17. N. Sogoshi, T. Wakabayashi, T. Momose, and T. Shida, *J. Phys. Chem. A* **101**, 522 (1997).
18. T. Momose, *J. Chem. Phys.* **107**, 7695 (1997).
19. T. Momose, M. Miki, T. Wakabayashi, T. Shida, M.C. Chan, S.S. Lee, and T. Oka, *J. Chem. Phys.* **107**, 7707 (1997).
20. T. Momose, H. Katsuki, H. Hoshina, N. Sogoshi, T. Wakabayashi, and T. Shida, *J. Chem. Phys.* **107**, 7717 (1997).
21. T. Momose, H. Hoshina, N. Sogoshi, H. Katsuki, T. Wakabayashi, and T. Shida, *J. Chem. Phys.* **108**, 7334 (1998).
22. M. Fushitani, N. Sogoshi, T. Wakabayashi, T. Momose, and T. Shida, *J. Chem. Phys.* **109**, 6346 (1998).
23. H. Hoshina, T. Wakabayashi, T. Momose, and T. Shida, *J. Chem. Phys.* **110**, 5728 (1999).
24. S. Tam, M.E. Fajardo, H. Katsuki, H. Hoshina, T. Wakabayashi, and T. Momose, *J. Chem. Phys.* **111**, 4191 (1999).
25. N. Sogoshi, Y. Kato, T. Wakabayashi, T. Momose, S. Tam, M.E. DeRose, and M.E. Fajardo, *J. Phys. Chem. A* **104**, 3733 (2000).
26. M.E. Fajardo and S. Tam, *J. Chem. Phys.* **108**, 4237 (1998).
27. S. Tam and M.E. Fajardo, *Rev. Sci. Instrum.* **70**, 1926 (1999).
28. R.J. Donnelly and C.F. Barenghi, *J. Phys. Chem. Ref. Data* **27**, 1217 (1998).
29. W. Wagner, A. Saul, and A. Pruss, *J. Phys. Chem. Ref. Data* **23**, 515 (1994).
30. F.D. Rossini, et al., *Selected values of physical and thermodynamic properties of hydrocarbons and related compounds*, Carnegie Press, Pittsburgh, PA (1953).
31. M.E. Fajardo and S. Tam, unpublished.
32. S. Tam, M. Macler, and M.E. Fajardo, *J. Chem. Phys.* **106**, 8955 (1997).
33. K. Kim, *J. Quant. Spectrosc. Radiat. Transfer* **30**, 413 (1983).
34. M.E. Fajardo, S. Tam, and T. Momose, unpublished.
35. G.L. Pollack, *Rev. Mod. Phys.* **41**, 48 (1960).
36. J.S. Buechner and H.J. Maris, *Phys. Rev. Lett.* **34**, 316 (1975).
37. C.L. Reynolds, Jr. and A.C. Anderson, *Phys. Rev. B* **14**, 4114 (1976).
38. C.L. Reynolds, Jr. and A.C. Anderson, *Phys. Rev. B* **15**, 5466 (1977).